

# Spin Polarization and Transport of Surface States in the Topological Insulators $\text{Bi}_2\text{Se}_3$ and $\text{Bi}_2\text{Te}_3$ from First Principles

Oleg V. Yazyev, Joel E. Moore, and Steven G. Louie

*Department of Physics, University of California, Berkeley, California 94720, USA and  
Materials Sciences Division, Lawrence Berkeley National Laboratory, Berkeley, California 94720, USA  
(Dated: December 7, 2010)*

We investigate the band dispersion and the spin texture of topologically protected surface states in the bulk topological insulators  $\text{Bi}_2\text{Se}_3$  and  $\text{Bi}_2\text{Te}_3$  by first-principles methods. Strong spin-orbit entanglement in these materials reduces the spin-polarization of the surface states to  $\sim 50\%$  in both cases; this reduction is absent in simple models but of important implications to essentially any spintronic application. We propose a way of controlling the magnitude of spin polarization associated with a charge current in thin films of topological insulators by means of an external electric field. The proposed dual-gate device configuration provides new possibilities for electrical control of spin.

PACS numbers: 73.20.-r, 75.70.Tj, 72.25.-b

The recently discovered three-dimensional topological insulators (TIs) [1–3] realize an unconventional electronic phase driven by strong spin-orbit interaction (SOI). The striking feature of these heavy-element materials is the existence of metallic Dirac fermion surface states characterized by an intrinsic spin helicity: the wavevector of the electron determines its spin state. A net spin density is thus produced upon driving a charge current at the surface of a TI. Considerable effort has been devoted recently to possible applications of this property of TIs to novel electronic devices, e.g., to spintronics [4] and topological quantum computing [5].

Understanding the properties of bulk TIs has mostly relied on few-band phenomenological models which treat the helical surface states as fully spin-polarized. However, one has to keep in mind that SOI entangles the spin and orbital momentum degrees of freedom thus reducing spin polarization. This is especially so for the currently investigated bulk TIs in which SOI is of electron-volt magnitude due to the presence of bismuth, the element with the largest atomic number  $Z$  which has stable isotopes [6, 7].

In this Letter, we apply first-principles methodology to study the topological surface states in  $\text{Bi}_2\text{Se}_3$  and  $\text{Bi}_2\text{Te}_3$ , the “second generation” materials which are currently considered as reference TIs [8, 9]. This approach is free of empirical parameters and treats topological surface states on an equal footing with other states across the electronic spectrum. The degree of spin polarization of the topological surface states is found to be significantly reduced in both bismuth materials, and this reduction will affect most spintronic applications of these materials. We use our results to propose a way of controlling the degree of spin polarization associated with the charge current in thin TI slabs by applying a transverse electric field. The proposed spintronic device is compared to a related proposal based on spin-polarized edge states in graphene [10] and to conventional semiconductor quantum wells.

First-principles electronic structure calculations have been performed within the density functional theory (DFT) framework employing the generalized gradient approximation (GGA) to the exchange-correlation functional [11]. Spin-orbit effects were treated self-consistently using fully relativistic norm-conserving pseudopotentials [12] acting on valence electron wavefunctions represented in the two-component spinor form [13]. A plane-wave kinetic energy cutoff of 35 Ry has been

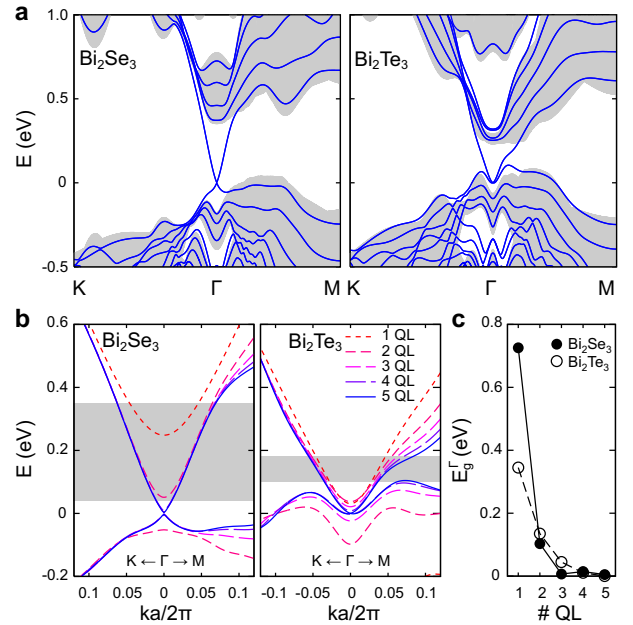


FIG. 1: (Color online). (a) Band structure of the 5 QL slabs of  $\text{Bi}_2\text{Se}_3$  and  $\text{Bi}_2\text{Te}_3$  (lines) superimposed with the projected band structure of the corresponding bulk materials (shaded areas). (b) Evolution of the surface state band dispersion in the vicinity of  $\Gamma$  point as a function of slab thickness. Shaded areas show the bulk band gaps. (c) Band gaps at the  $\Gamma$  point induced by the interaction between the surface states as a function of slab thickness.

employed for the wavefunctions. Surface states in  $\text{Bi}_2\text{Se}_3$  and  $\text{Bi}_2\text{Te}_3$  bulk TIs were investigated using (111) slab models of varying thickness (1–5 quintuple layers (QL) equivalent to  $\sim 1\text{--}5\text{ nm}$ ) with atomic positions taken from experimental data using a supercell geometry [14]. Such an approach has already been used previously [8, 15, 16]. The effects of applied electric field were simulated by adding a sawtooth-like potential profile with a constant slope in the slab region [17]. The PWSCF code of the QUANTUM-ESPRESSO distribution [18] was used in the present study.

We start our discussion by considering the band structure of the bulk materials and slabs of finite thickness. Figure 1(a) shows the band structure of 5 QL slabs superimposed with the bulk band structure projected onto the surface Brillouin zone (BZ). The band structures of the slab and bulk systems are aligned by matching the potential in “bulk-like” region of the slab to the bulk potential. Within the DFT-GGA approach the band gaps of  $\text{Bi}_2\text{Se}_3$  and  $\text{Bi}_2\text{Te}_3$  are 0.31 eV and 0.08 eV, respectively. The value for  $\text{Bi}_2\text{Se}_3$  is in good agreement with another theoretical report (0.32 eV [19]) and experimental data (0.35 eV [20]), a fortuitous result considering the well-known tendency of DFT to underestimate band gaps [21]. The calculated band gap for  $\text{Bi}_2\text{Te}_3$  is consistent with another first-principles result [22] and is smaller than 0.165 eV measured experimentally [23].

The topological surface states are distinguished in the slab band structures as the “Dirac cone” feature at the  $\Gamma$  point, especially clear in the case of  $\text{Bi}_2\text{Se}_3$ . The Dirac point energies  $E^D$  (below,  $E^D = 0\text{ eV}$  is set for convenience) are situated 0.04 eV and 0.10 eV below the corresponding bulk valence band maxima (VBM) within DFT-GGA. In slab geometry, the surface state bands are doubly degenerate with corresponding surface states of the opposite spin helicities localized at the opposite surfaces. The topological surface bands in bulk TIs do not respect electron-hole symmetry, and the Fermi velocity  $v_F$  shows rather complex behavior. At the VBM energy the calculated  $v_F = 4.6 \times 10^5\text{ m/s}$  in  $\text{Bi}_2\text{Se}_3$  agrees with experimental results [8]. The magnitude of  $v_F$  increases with increasing energy and reaches  $6.4 \times 10^5\text{ m/s}$  at the bulk conduction band minimum (CBM) energy for wavevectors along the  $\Gamma$ –K direction. However, along the  $\Gamma$ –M direction there is a noticeable softening ( $v_F = 3.8 \times 10^5\text{ m/s}$ ) due to the hexagonal warping effect. The surface-state band of  $\text{Bi}_2\text{Te}_3$  shows stronger anisotropy in agreement with experimental observations of a strong hexagonal warping [23]. At  $E = 0.1\text{ eV}$ ,  $v_F = 4.1 \times 10^5\text{ m/s}$  ( $3.3 \times 10^5\text{ m/s}$ ) along the  $\Gamma$ –K ( $\Gamma$ –M) direction. The variation of  $v_F$  along the  $\Gamma$ –K direction is weak, while along the  $\Gamma$ –M direction it reduces to  $1.2 \times 10^5\text{ m/s}$  at the CBM energy.

Figure 1(b) illustrates the evolution of the surface band dispersion as a function of slab thickness. Vacuum potential alignment is used for the comparison of the slab sys-

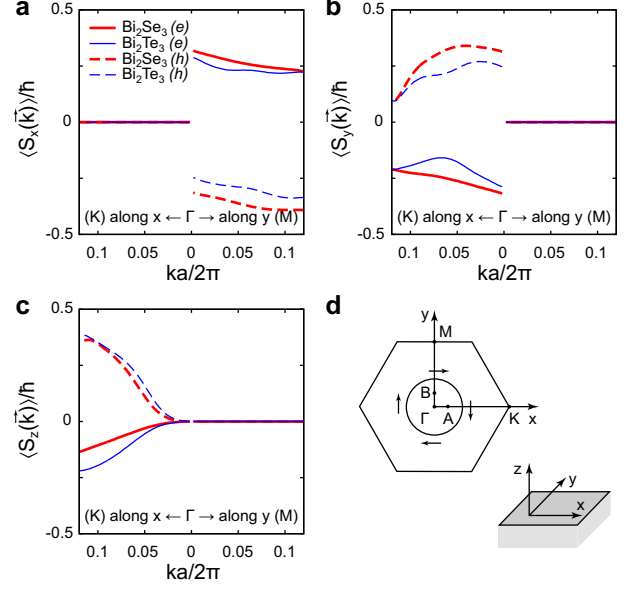


FIG. 2: (Color online). (a–c) Expectation values of the spin operators  $\langle S_\alpha(\vec{k}) \rangle$  ( $\alpha = x, y, z$ ) for the topological surface states along the selected path (A– $\Gamma$ –B) in momentum space (d) for 4 QL slabs of  $\text{Bi}_2\text{Se}_3$  and  $\text{Bi}_2\text{Te}_3$ . Electron (solid lines) and hole (dashed lines) surface state bands are distinguished. The surface normal corresponds to  $z$  direction. Coordinate system is right-handed (d, inset).

tems. In thin slabs, the interactions between the states localized at the opposite surfaces opens a gap ( $E_g^\Gamma$ ) at the Dirac point. The magnitude of the gap decays rapidly with increasing slab thickness [Fig. 1(c)], and the values are in quantitative agreement with other first-principles results [15]. The dispersion of the surface state bands is essentially converged by 3 QL and 4 QL in  $\text{Bi}_2\text{Se}_3$  and  $\text{Bi}_2\text{Te}_3$ , respectively. On the other hand, in thin slabs, quantum confinement pulls apart the bulk valence and conduction band edges thus increasing the energy range in which topological surface states are separated from bulk-like states.

The striking feature of the surface states of TIs is the helicity of the spin polarization vector  $\vec{P}(\vec{k}) = (2/\hbar)[\langle S_x(\vec{k}) \rangle, \langle S_y(\vec{k}) \rangle, \langle S_z(\vec{k}) \rangle]$  along the constant energy contours. Here, the expectation values of spin operators  $\langle S_{\alpha i}(\vec{k}) \rangle = (\hbar/2)\langle \psi_i(\vec{k}) | \sigma_\alpha | \psi_i(\vec{k}) \rangle$  ( $\alpha = x, y, z$ ), where  $\psi_i(\vec{k})$  are the two-component spinor wavefunctions,  $\sigma_\alpha$  the corresponding Pauli matrices. The recent spin- and angle-resolved photoemission spectroscopy (spin-ARPES) experiments have indeed indicated a one-to-one locking of the momentum and the direction of spin polarization vector pointing along  $(\vec{k} \times \vec{z})$  [24]. First-principles results have confirmed this picture [25]. However, we would like to stress that the magnitude of spin-polarization  $\vec{P}(\vec{k})$  can be reduced from the maximum value of 100% since the electron spin quantum number is no longer conserved in systems with SOI [26]. Spin-orbit

coupling leads to Bloch states that are not separately spin eigenstates but instead have entanglement between their spin and orbital parts. An illustration of the effects of SOI on the spin projections in the case of bcc iron is given in Ref. 27. Such effects are expected to be especially pronounced in bismuth materials where the exceptionally strong SOI, of the order of an electron-volt [6, 7], would make the surface states a mixture of bulk states from a broad energy range.

Figures 2(a)–2(c) show the calculated expectation values of the spin operators  $\langle S_\alpha(\vec{k}) \rangle$  for both electron and hole states of the surface band in Bi<sub>2</sub>Se<sub>3</sub> and Bi<sub>2</sub>Te<sub>3</sub> along  $x$  and  $y$  directions in momentum space [see Fig. 2(d) for definition]. The surface normal corresponds to  $z$  direction and the standard convention of the right-handed coordinate system applies [Fig. 2(d), inset]. We find that the spin polarization vectors are aligned preferentially in the  $xy$  plane and the helicity is left (right) handed for the conduction or above  $E^D$  (valence or below  $E^D$ ) bands. This is consistent with previous experimental measurements [24] and theoretical calculations [25]. However, the magnitudes of the spin projections are significantly reduced with respect to the nominal value of  $\pm\hbar/2$ . Close to the  $\Gamma$  point we find  $\sim 50$ – $60\%$  spin-polarization for both materials. Its magnitude tends to decrease with increasing energy. The magnitude of spin projections close to the Dirac point appears to be rather insensitive to the slab thickness (not shown here). We have studied the microscopic origin of the reduction of spin polarization and find that the surface Bloch state is a complex superposition of different spin directions on different atoms; hence the reduction of the spin polarization cannot simply be understood in a tight-binding picture built from atomic eigenstates of total angular momentum. A remarkable out-of-plane spin projection  $\langle S_z(\vec{k}) \rangle$  develops in the  $\Gamma$ – $K$  direction as it was recently ascribed to the hexagonal warping effect [28]. In general, we find somewhat larger reduction of the spin polarization and more pronounced hexagonal warping effects on the out-of-plane spin projection in the case of heavier Bi<sub>2</sub>Te<sub>3</sub>.

From the point of view of technological applications, an attractive feature of the TI materials is the intrinsic spin polarization of the current carried by the topological surface states. For charge carriers (electrons) moving along  $y$  direction ( $k_y > 0$ ) the transferred spin polarization (i.e. spin polarization of the current injected through a transparent tunneling barrier) is along  $x$  axis and its geometric average  $\langle P_x(E) \rangle = (\pi/4)|\vec{P}(E)|$ . We define  $\langle P_x(E) \rangle = \frac{\int d\vec{k} v_y(\vec{k}) P_x(\vec{k}) \delta(E - E_{\vec{k}})}{\int d\vec{k} v_y(\vec{k}) \delta(E - E_{\vec{k}})}$ , where  $v_y(\vec{k})$  is the carrier velocity along the transport direction. In the discussed materials  $\langle P_x(E) \rangle \approx 50\%$  and shows only weak dependence on  $E$ , but changes its sign when the character of charge carriers (electrons vs. holes) changes. Moreover, in TI films the opposite spin helicities of the charge carriers at the opposite surfaces would result in

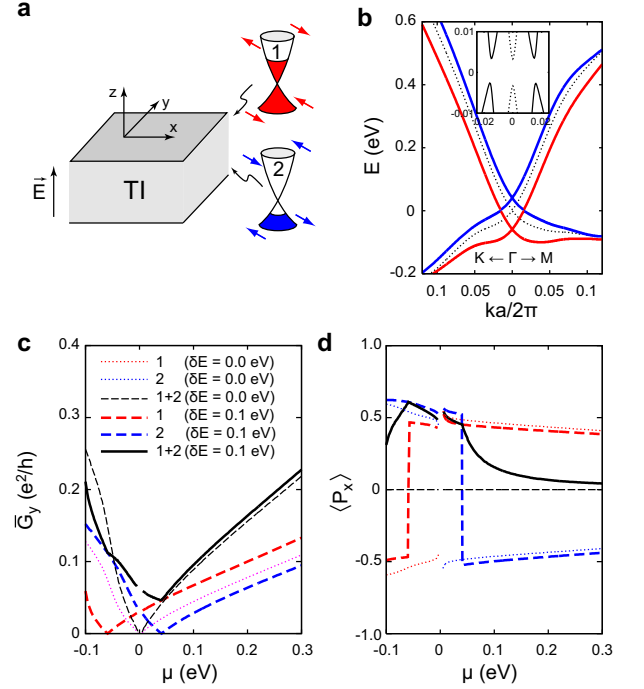


FIG. 3: (Color online). (a) Illustration of the effect of electric field  $\vec{E}_{\text{ext}}$  applied across a thin slab of bulk TI. The filling of the two surface state bands and the corresponding spin textures for electrons and holes are shown. (b) Splitting of the surface state bands by applied electric field ( $\delta E = 0.1$  eV, solid lines) in a 3QL slab of Bi<sub>2</sub>Se<sub>3</sub> compared to the band dispersion at zero field (dotted lines). The inset shows a close-up view of band gaps at the charge neutrality point. (c) Individual (surfaces 1 and 2) and total ballistic conductances in  $y$  direction per device width,  $\bar{G}_y$ , and (d) spin polarization along  $x$  axis,  $P_x$ , for  $\delta E = 0.1$  eV and  $\delta E = 0$  eV as a function of chemical potential  $\mu$  ( $\mu = 0$  eV corresponds to the charge neutrality point). The symbols have same meaning in (c) and (d).

zero net spin polarization.

We anticipate that improved control over spin transport can be achieved in few-nanometer thick slabs of Bi<sub>2</sub>Se<sub>3</sub> and Bi<sub>2</sub>Te<sub>3</sub> which can be produced by molecular-beam epitaxy [29, 30], vapor deposition [31, 32], or exfoliation [33]. Tuning the chemical potential  $\mu$  in such thin slabs by gating has already been achieved [32]. Similarly to bilayer graphene [34], the TI slabs are characterized by imperfect screening due to the semimetallic nature of the surface states. Thus, in the dual-gate device configuration or by coupling TI thin films to a ferroelectric substrate it is also possible to control splitting  $\delta E = E_2^D - E_1^D$  between the Dirac point energies  $E_1^D$  and  $E_2^D$  of the two surface bands given with respect to the common chemical potential [Fig. 3(a)]. Such splitting of  $\sim 0.1$  eV produced by the SiC substrate has been reported for Bi<sub>2</sub>Se<sub>3</sub> thin films [29]. Close to the Dirac point, the response of a thin TI film of thickness  $d$  to an applied electric field  $\vec{E}_{\text{ext}}$  is expected to be dominated by the bulk screening

contribution,  $\delta E = |\vec{E}_{\text{ext}}|d/\epsilon_{\parallel}(0)$ . The static dielectric constant along  $c$ -axis  $\epsilon_{\parallel}(0) = 75$  for  $\text{Bi}_2\text{Te}_3$ ; probably smaller for  $\text{Bi}_2\text{Se}_3$  [35]. Figure 3(b) shows the surface state band dispersion calculated from first-principles for a 3 QL slab of  $\text{Bi}_2\text{Se}_3$  under applied electric field  $\vec{E}_{\text{ext}}$  resulting in  $\delta E = 0.1$  eV (here,  $\vec{E}_{\text{ext}} = 1.72$  V/nm for the supercell dimension along  $z$  axis equal to 4.36 nm). The conical surface state bands shift rigidly with respect to each other while the bulk-like states (not shown) remain practically unaffected by the applied field. Figure 3(c) shows the individual surface state Sharvin conductances along  $y$  direction (i.e. the number of ballistic channels per device width along  $x$  axis given in the units of lattice constant  $a$ ),  $\bar{G}_y^1$  and  $\bar{G}_y^2$ , and their sum  $\bar{G}_y$ .

The applied field lifts the semi-metallic conductance close to the charge neutrality point. Note that for both  $\delta E = 0.0$  eV and  $\delta E = 0.1$  eV there is a 0.006 eV band gap opening at the charge-neutrality point due to the hybridization of the surface states localized on the opposite sides of the thin film. For  $E_1^D < \mu < E_2^D$  the charge carriers are electrons (holes) at surface 1 (2). Importantly, in this range of  $\mu$  the transferred spin polarization along  $x$  direction is of the same sign for both surface conduction channels [Fig. 3(d)]. The total transferred spin polarization  $\langle P_x \rangle$  is non-zero in the case of applied electric field. We note that these conditions are away from the symmetric situation that has been argued to lead to exciton condensation [36]. The magnitude of  $\langle P_x \rangle$  can be tuned by changing  $\mu$  and achieves maximum its value  $\langle P_x \rangle = 0.608$  at  $\mu = E_1^D$ . The sign of  $\langle P_x \rangle$  can be changed by simply inverting the direction of  $\vec{E}_{\text{ext}}$ . That is, the dual-gate device based on a thin slab of TI permits to control independently both the conductance and the degree transferred spin polarization of injected current in a broad range, certainly a highly attractive opportunity for spintronics applications.

Such spintronic device can be compared to another theoretical proposal which realizes electric control over spin transport. This device based on zigzag graphene nanoribbons relies on the peculiar spin-polarized edge states of topologically-trivial origin [10]. While in TI slabs the degree of transmitted spin-polarization is limited by the SOI and by the geometric average prefactor  $\pi/4$ , the localized states at the zigzag edges of graphene are always 100% spin-polarized. On the other hand, the degree of spin-polarization can be continuously tuned in the TI slabs. The direction of  $\vec{P}$  is fixed with respect to the current direction at the TI surfaces, while graphene-based magnetic systems are characterized by low magnetic anisotropy as a result of very weak SOI in carbon and by relatively short spin correlation length [37, 38].

In a more general context, it is instructive to compare the spin transport effects at the TI surfaces to those in other 2D systems, e.g. to the corresponding effect induced by Rashba SOI in a 2D electron gas, where a

current also induces a spin density. The basic difference is that the Rashba coupling leads to two Fermi surfaces with opposite spin directions at each momentum, and the resulting current-induced spin densities nearly cancel if the SOI is small. A single TI surface has only *one* spin state at each momentum and hence no cancellation. Quantitatively, we write the Rashba SOI as  $\alpha\hbar(\vec{k} \times \sigma)_z$  where  $\alpha$  has units of velocity and  $\sigma$  are Pauli matrices. The cancellation between Fermi surfaces reduces the spin density by a factor of order  $\alpha/v_F$  compared to a model TI surface with a single Dirac cone, where  $v_F$  is the Fermi velocity. Taking one example,  $\alpha$  in a InGaAs/InAlAs quantum wells was measured to be  $7\text{--}14 \times 10^3$  m/s [39], more than an order of magnitude less than  $v_F \sim 5 \times 10^5$  m/s in  $\text{Bi}_2\text{Se}_3$  and  $\text{Bi}_2\text{Te}_3$  [8, 23].

We would like to thank E. Kioupakis, J. Orenstein and C. Jozwiak for discussions. This work was supported in part by National Science Foundation Grants No. DMR07-05941 and DMR08-04413. O. V. Y. is recipient of a Swiss National Science Foundation fellowship (grant No. PBELP2-123086) and partially supported by the Director, Office of Science, Office of Basic Energy Sciences, Division of Materials Sciences and Engineering Division, U.S. Department of Energy under Contract No. DE-AC02-05CH11231. Computational resources have been provided by TeraGrid (Kraken).

- 
- [1] L. Fu, C. L. Kane, and E. J. Mele, Phys. Rev. Lett. **98**, 106803 (2007).
  - [2] J. E. Moore and L. Balents, Phys. Rev. B **75**, 121306 (2007).
  - [3] D. Hsieh *et al.*, Nature (London) **452**, 970 (2008).
  - [4] I. Garate and M. Franz, Phys. Rev. Lett. **104**, 146802 (2010).
  - [5] L. Fu and C. L. Kane, Phys. Rev. Lett. **100**, 096407 (2008).
  - [6] P. Carrier and S.-H. Wei, Phys. Rev. B **70**, 035212 (2004).
  - [7] K. Wittel and R. Manne, Theor. Chim. Acta **33**, 347 (1974).
  - [8] Y. Xia *et al.*, Nature Phys. **5**, 398 (2009).
  - [9] H. Zhang *et al.*, Nature Phys. **5**, 438 (2009).
  - [10] Y.-W. Son, M. L. Cohen, and S. G. Louie, Nature (London) **444**, 347 (2006).
  - [11] J. P. Perdew, K. Burke, and M. Ernzerhof, Phys. Rev. Lett. **77**, 3865 (1996).
  - [12] A. Dal Corso and A. Mosca Conte, Phys. Rev. B **71**, 115106 (2005).
  - [13] L. Nordström and D. J. Singh, Phys. Rev. Lett. **76**, 4420 (1996); T. Oda, A. Pasquarello, and R. Car, Phys. Rev. Lett. **80**, 3622 (1998); R. Gebauer *et al.*, Phys. Rev. B **61**, 6145 (2000).
  - [14] M. L. Cohen, M. Schlüter, J. R. Chelikowsky, and S. G. Louie, Phys. Rev. B **12**, 5575 (1975).
  - [15] C.-X. Liu *et al.*, Phys. Rev. B **81**, 041307 (2010).
  - [16] S. Eremeev, Y. Koroteev, and E. Chulkov, JETP Lett. **91**, 387 (2010).
  - [17] K. Kunc and R. Resta, Phys. Rev. Lett. **51**, 686 (1983);

- R. Resta and K. Kunc, Phys. Rev. B **34**, 7146 (1986).
- [18] P. Giannozzi *et al.*, J. Phys.: Condens. Matter **21**, 395502 (2009).
- [19] P. Larson *et al.*, Phys. Rev. B **65**, 085108 (2002).
- [20] J. Black *et al.*, J. Phys. Chem. Solids **2**, 240 (1957).
- [21] M. S. Hybertsen and S. G. Louie, Phys. Rev. B **34**, 5390 (1986).
- [22] S. J. Youn and A. J. Freeman, Phys. Rev. B **63**, 085112 (2001).
- [23] Y. L. Chen *et al.*, Science **325**, 178 (2009).
- [24] D. Hsieh *et al.*, Nature (London) **460**, 1101 (2009).
- [25] W. Zhang, R. Yu, H.-J. Zhang, X. Dai, and Z. Fang, New J. Phys. **12**, 065013 (2010).
- [26] C. L. Kane and E. J. Mele, Phys. Rev. Lett. **95**, 146802 (2005).
- [27] X. Wang, J. R. Yates, I. Souza, and D. Vanderbilt, Phys. Rev. B **74**, 195118 (2006).
- [28] L. Fu, Phys. Rev. Lett. **103**, 266801 (2009).
- [29] Y. Zhang *et al.*, Nature Phys. **6**, 584 (2010).
- [30] Y.-Y. Li *et al.*, Adv. Mater. **22**, 4002 (2010).
- [31] D. Kong *et al.*, Nano Lett. **10**, 329 (2010).
- [32] D. Kong *et al.*, Nano Lett. **10**, 2245 (2010).
- [33] D. Teweldebrhan, V. Goyal, and A. A. Balandin, Nano Lett. **10**, 1209 (2010).
- [34] Y. Zhang *et al.*, Nature (London) **459**, 820 (2009).
- [35] O. Madelung, U. Rössler, and M. Schulz (eds.), SpringerMaterials – The Landolt-Börnstein Database (<http://www.springermaterials.com>).
- [36] B. Seradjeh, J. E. Moore, and M. Franz, Phys. Rev. Lett. **103**, 066402 (2009).
- [37] O. V. Yazyev and M. I. Katsnelson, Phys. Rev. Lett. **100**, 047209 (2008).
- [38] O. V. Yazyev, Rep. Prog. Phys. **73**, 056501 (2010).
- [39] J. Nitta, T. Akazaki, H. Takayanagi, and T. Enoki, Phys. Rev. Lett. **78**, 1335 (1997).